‘Increased Energy in Stable Dry-band Arcs Due to Length Compression‘

X. Zhang, S. M. Rowland and V. Terzija

IEEE Transactions on Dielectrics and Electrical Insulation, Vol. 17, Issue 2, pp. 473-480, April 2010

Digital Object Identifier: 10.1109/TDEI.2010.5448103

Increased Energy in Stable Dry-band Arcs Due to Length Compression

X. Zhang, S. M. Rowland and **V. Terzija**
School of Electrical and Electronic Engineering
The University of Manchester
PO Box 88, Sackville Street, Manchester, M60 1QD, United Kingdom

ABSTRACT

The occurrence of dry-band arcs on outdoor composite insulators can degrade the polymeric materials' surface and ultimately may lead to insulator failure. The degradation processes are generally considered as aging effects occurring over long periods of time, from years to decades. In this paper, it is shown that if a stable dry-band arc is physically compressed in length by external forces, such as electrolyte deformation due to wind or gravity, the arcing activities will become more severe. This in turn, may accelerate the degradation into a short time-frame hazard. A series of experiments are carried out to investigate the electrical characteristics of the arcs as they become compressed. In this case experiments are performed on silicone rod insulators at controlled angles to the horizontal. Rapid aging is observed after such events. Measurements of arcing period, peak current, and arc resistance during the arcing compression process are analyzed. Based on the experiments, a 'Double Sinusoidal Model' is developed to simulate the current-voltage characteristics of dry-band arcing during its compression. Both experiment and simulation show that arc power, arc energy and corresponding energy density will dramatically increase if arc compression occurs, which may lead to more rapid and serious damage on composite insulator surfaces than is experienced otherwise. It is suggested that aggressive erosion events may occur in short periods of time within extended test regimes or entire service histories.

Index Terms — **Composite insulator, silicone rubber, aging, NCI. dry-band arc compression, model, arc energy.**

1 INTRODUCTION

IN both service and experimental conditions, electrical discharges such as dry-band arcings may develop on insulator surfaces due to electric fields, the presence of moisture, low surface hydrophobicity and pollution [1]. Dry-band arcing is one mechanism responsible for the chemical changes to the surfaces of polymer insulators, which may lead to hydrophobicity loss, erosion of the surface, and even penetration revealing the fibreglass core and ultimately causing mechanical failure of the insulator [2-5].

Dry-band arc currents are normally limited to the order of milliamps due to the resistance presented by the rest of the insulator surfaces. If currents exceed 100 mA, flashover becomes a possibility. Dry-band arc resistant materials have been developed over the years which are able to limit resulting degradation and erosion [6]. Therefore, the deterioration from discharges including dry-band arcing is generally considered as a long-term aging effect on good quality composite insulators, and these materials can withstand dry-band arcs for many hundreds or even thousands of hours in laboratory salt-fog tests.

As a result of research on accelerated damage on ADSS (all dielectric self-supporting) cables designed for high voltage environments [7-8], a novel view has been proposed that accelerated degradation on insulator surfaces could be possible if a dry-band arc is physically compressed in length. Such an 'arc-compression' event can result from the movement of moisture at the edge of a stable dry-band over which an arc is struck. The arc contributes to the likelihood of moisture movement because it reduces the surface tension of the water at the arc roots. In this paper it is shown that dry-band arc compression results in more energetic arcs and such compressed arcs can degrade insulator surfaces much quicker than the normal gradual degradation expected. As a result it is proposed that local deep erosion patterns seen after extended tests or periods of service can be due to rare arc-compression events rather than gradual erosion.

A series of investigations for dry-band arcing characteristics are reported in [9-13]. Those studies were based on horizontal samples where the dry-band arcs could grow to their natural full length. Inclined plane testing with contaminant flowing down a slope to an arcing location [14] naturally compresses

Manuscript received on 12 May 2009, in final form 17 July 2009.

the arc and changes the arcing properties in comparison to the horizontal situation. This is understood to be a more aggressive test. The proposed mechanism in this paper lies somewhere between these two situations.

During the proposed mechanism [8], thermal and moisture balances are reached allowing formation of a stable dry-band arc with repeatable electrical behavior in every power cycle (Figure 1a). When the sample is inclined (Figure 1b), the upper water film and lower water film, whose edges are at the dry-band boundaries, will tend to move down the insulator core due to gravity. The upper film tends to move faster because of the feeding of moisture from the rod above it and because of the breakdown of surface tension due to the arc. When moisture addition is heavy, droplets tend to congregate underneath the rod, which accelerates this movement. In very heavy wetting conditions droplets running through the dry-band can extinguish the arc permanently or temporarily. A dry-band can gradually move down the rod by this means until the lower water film is replaced by the immobile metallic fitting. The metallic fitting then becomes an immovable lower edge of the dry-band. In the meantime, the upper water film can still move downwards. Following this, two possible situations may occur:

A) A single stable dry-band arc remains but the arc length is physically compressed in length. The length of the arc is reduced to extinction unless a new balance is achieved.

B) The dry-band arc becomes unstable and one or more dry-bands are initiated elsewhere on the rod as the original dry-band is swamped and the arc extinguished.

Such movement of moisture can result from prevailing winds on outdoor horizontal rod insulators (or ADSS cables) [8]. However, for experimental expediency and control, the process has been investigated using sloping samples in the laboratory. Further work will be required to consider the likelihood and frequency of such occurrences in service conditions.

2 EXPERIMENTAL

2.1 TEST ARRANGEMENT

Figure 2 illustrates the design of the inclined sample test. The 300 mm long sample tested was a 22 mm diameter rod, consisting of 4 mm radial thickness commercial grade silicone rubber on a glass-reinforced polymer core. A remotely controlled pulley system lifts one end of sample to create an incline. The silicone rubber surface was uniformly roughened with abrasive paper to reduce its surface hydrophobicity to encourage rapid formation of continuous water films on the surface and so the initial formation of a stable dry-band arc.

Electrodes, separated by 200 mm, were formed by wrapping copper strip tightly around the rod. The water film was created by the precipitation of surrounding salt-fog throughout the test, with a conductivity of 16,000 μS/cm, and the precipitation rate in the chamber was 0.4±0.1 l/m^3/hr.

A water resistor of 10 MΩ was used throughout the

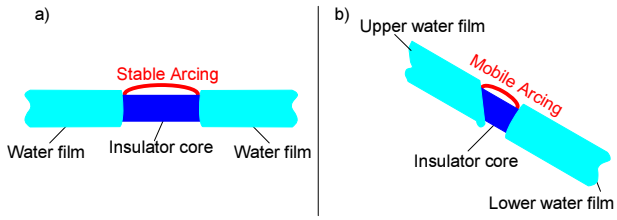

Figure 1. Dry-band arcing compression on insulator core between two water films.

experiment to limit the leakage current. The data acquisition system was a National Instrument Labview system with a voltage divider of 10,000:1 to determine the voltage waveform across the rod sample, and a measurement resistor of 1 kΩ to record current. The voltage and current signals were stored in a PC with a sample rate of 40 kHz.

2.2 TEST PROCEDURE

I. The transformer voltage was fixed at 17.4 kV throughout the tests. The sample was set to the horizontal position in the salt-fog. It took about an hour to obtain a single stable arc on the material surface.

II. The sample was lifted to 5°. The length of arc was reduced reaching equilibrium after 30 minutes, at which time its new length was recorded. Normally the arc gradually moved down the rod until it reached the lower electrode.

III. The sample was lifted to 10°. 30 minutes was allowed for equilibrium to be reached. Then the sample was inclined to 15°, 20°, 25°, 30°, 35° with 30 minutes intervals between each slope angle, measurements being taken accordingly.

IV. When the slope angle reached 40°, the arcing was extinguished. At this stage the leakage current waveform became sinusoidal, in phase with the supply voltage.

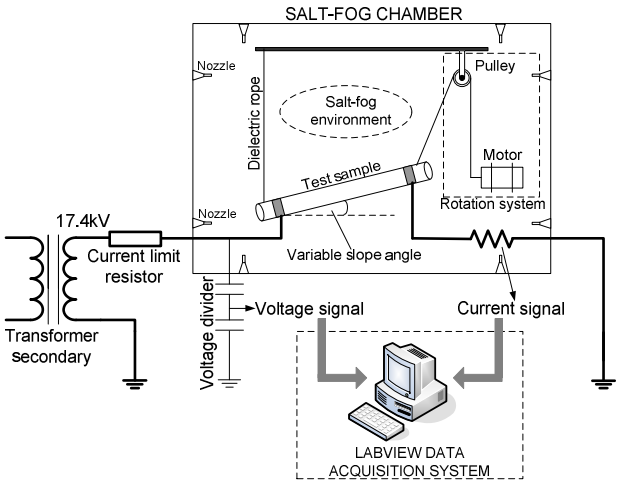

Figure 2. The test arrangement.

2.3 RESULTS

Voltage and current signals were obtained for 5° slope increments between the horizontal and 40°, along with associated arc lengths. Figure 3 gives examples of test results. Detailed results are presented in Section 3. Arc intensity can visibly be seen to increase as the arc is reduced in length, becoming whiter in colour. This is particularly evident for very short arcs as the arc is extinguished, as the rod angle is increased above 35°.

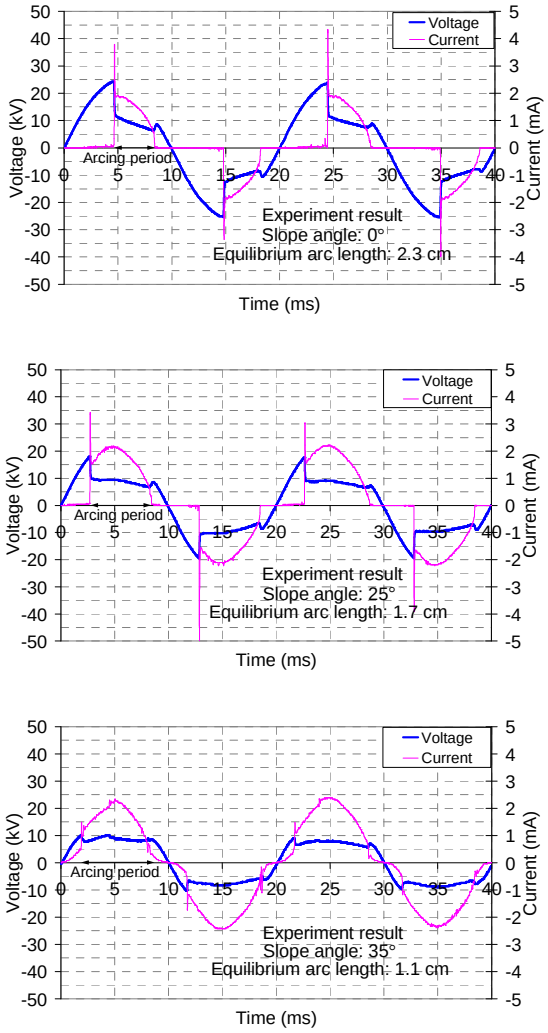

Figure 3. Experimental results of current and voltage traces for slope angles of 0°, 25° and 35°.

3 MODELLING

3.1 DOUBLE SINUSOIDAL MODEL

A 'double sinusoidal model' can be used to analyze the electrical characteristics of dry-band arcing during the arc-compression process. A limited model was in introduced elsewhere [15], and this is now developed to allow variation in peak current with arc length. In the model, two sinusoidal waves are introduced to simulate the experimental current and voltage characteristics, shown in Figure 4. In each half-cycle three periods are identified: the pre-arcing period, the arcing period and the post-arcing period [16]. For simplification, the arc is represented as having a flat voltage during its existence. The model is represented by the equations from these three periods as:

Pre-arcing period: $0 < t < t_1$

$$i_a(t)=0 \quad (1)$$

$$u_a(t)=\sqrt{2}U_a \sin\omega_u t \quad (2)$$

Arcing period: $t_1 < t < t_2$

$$i_a(t)=\sqrt{2}I_a \sin\omega_i [t-(\frac{\pi}{\omega_u}-t_2)] \quad (3)$$

$$u_a(t)=U_0 \quad (4)$$

Post-arcing period: $t_2 < t < 10$ ms

$$i_a(t)=0 \quad (5)$$

$$u_a(t)=\sqrt{2}U_a \sin\omega_u t \quad (6)$$

where: $i_a(t)$ and $u_a(t)$ are simulated current (mA) and voltage (kV) curves. I_a and ω_i are the rms value (mA) and angular frequency (rad/ms) of the current sinusoidal wave. U_a and ω_u are the rms value (kV) and angular frequency (rad/ms) of the voltage sinusoidal wave. U_0 is the arc voltage (kV) during the arcing period. t_1 is the arc ignition time (ms). t_2 is the arc extinction time (ms).

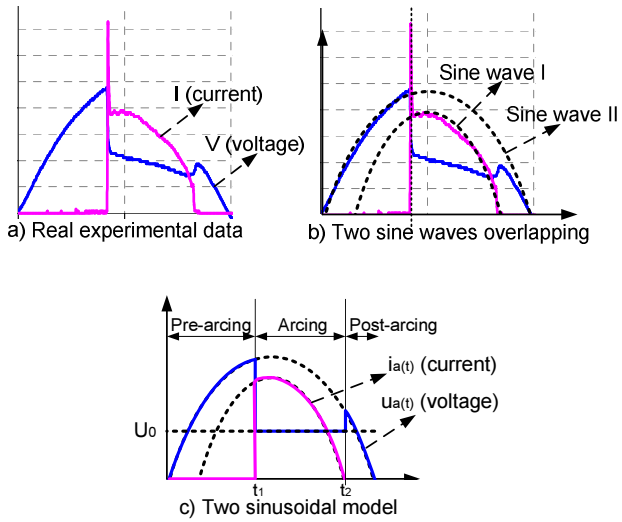

Figure 4. Double sinusoidal model to simulate I-V curves for dry-band arc.

3.2 ARC CHARACTERISTICS WITH SLOPE ANGLE

At each slope angle, the experiment data from four half-cycles (400 points per half-cycle) were used to analyze arc length, arc period, breakdown voltage and arc current peak.

Figure 5 shows the relationship between arc length and slope angle. In this and following figures, error bars indicate standard deviations of measurement taken. For every half cycle, pictures were extracted frame-by-frame from video images and Vistametrix software used to extract the arc length

from the picture. As arc length varies during a half cycle, the maximum arc length was used for analysis. In the horizontal position (0° slope), the arc grows without external forces moving the two water films at the dry-band edge. Following the increase of slope angle, the dry-band length was reduced. When the slope angle reached around 40°, the dry-band area has been entirely submerged by the upper water film, extinguishing the arcing activity.

The arcing period is defined as the period from arc ignition time t_1 to arc extinction time t_2. Figure 6 shows the experimental results of arcing period against different arc lengths. As the arc is reduced in length, the arcing period becomes longer. This is due to the change of arc ignition time with different arc length. Shorter dry-bands require lower breakdown voltages, this in turn brings forward the time for arc ignition. However, the arc extinction time remains unchanged because the arc extinction voltages are roughly the same in each slope angle case. Thus t_2 is a constant parameter in the model, independent of dry-band length and rod inclination.

The breakdown voltage is defined here as the instantaneous voltage at arc ignition. As the arc is compressed in length, the breakdown voltage reduces linearly with dry-band length from 0° to 35° (Figure 7). The reason for this trend is that dry-band arc compression results in a shorter distance of air gap between the two water layers, requiring a lower threshold voltage to break down the gap for arc ignition.

The peak arcing current for each dry-band length is shown in Figure 8. This relationship shows that the arc current peak rises linearly as arc length decreases. The extreme condition occurs at the slope angle of 40°, where the dry-band has been swamped by the higher water film running down the rod, leading to a maximum leakage current, limited only by the external circuit's water resistor.

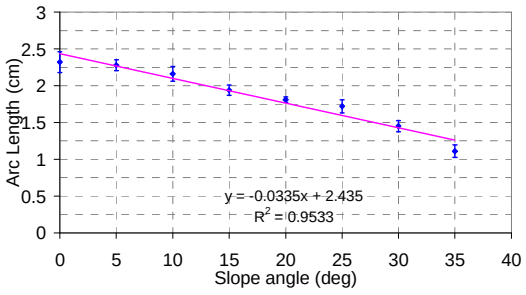

Figure 5. The relationship between arc length and slope angle.

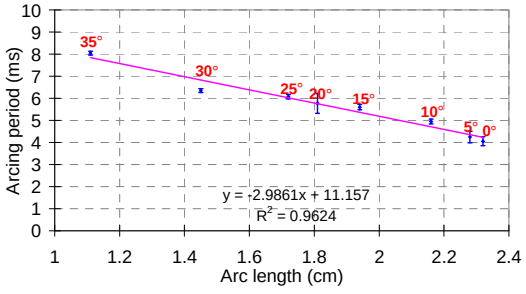

Figure 6. The relationship between arcing period and arc length.

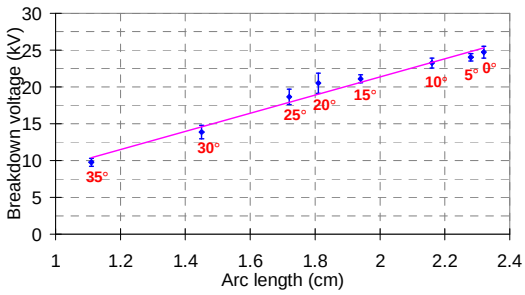

Figure 7. The relationship between breakdown voltage and arc length.

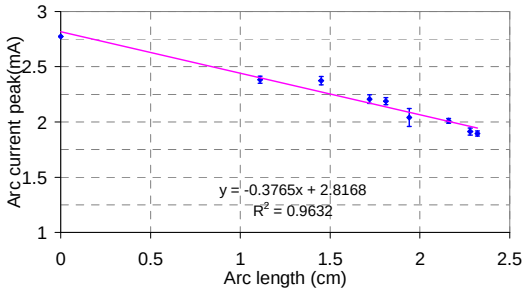

Figure 8. The relationship between arc current peak and arc length.

3.3 ARC PARAMETERISATION

The relationship between arc length, arcing period, arc ignition time and arc extinction time is established empirically by analyzing experimental result as:

$$T_{arc}=t_2-t_1=-2.99L_a+11.16 \quad (7)$$

$$t_1=f(L_a,t_2)=t_2+2.99L_a-11.16 \quad (8)$$

where: T_{arc} is the arcing period, t_1 is the ignition time, t_2 is the extinction time (all in ms) and L_a is the arc length (cm).

The relationship between arc current peak and arc length is represented as:

$$\sqrt{2}I_a=-0.3765L_a+2.8168 \quad (9)$$

$$I_a=\frac{1}{\sqrt{2}}\times(-0.3765L_a+2.8168)=-0.27L_a+1.99 \quad (10)$$

where I_a is the rms value (mA) of simulated current sinusoidal wave.

A double sinusoidal model of I-V curves for the dry-band arc compression in every half cycle is obtained by combining equations (1-8) together with the sign function as follows:

$$i_a(t)=\sqrt{2}I_a\sin\omega_i[t-(\frac{\pi}{\omega_u}-t_2)]\times\frac{1-\text{sign}[(t-t_2-2.99L_a+11.16)(t-t_2)]}{2} \quad (11)$$

$$u_a(t)=\sqrt{2}U_a\sin\omega_u t\times\frac{1+\text{sign}[(t-t_2-2.99L_a+11.16)(t-t_2)]}{2}+U_0\times\frac{1-\text{sign}[(t-t_2-2.99L_a+11.16)(t-t_2)]}{2} \quad (12)$$

where: $i_a(t)$ and $u_a(t)$ are simulated current (mA) and voltage

(kV) curves, for $0 < t < 10$ (ms).

Table 1 summarizes the parameters for the double sinusoidal model, estimated from experimental data. By observing the change in I-V curves with different arc lengths, it is determined that the U_a, U_0, ω_i, ω_u, and t_2 are constant, while t_1, I_a and L_a are variable with dry-band length. t_1 is represented by equation (8) and I_a is represented by equation (10). L_a varies representing different arc compression situations.

3.4 SIMULATION RESULTS

By introducing the model parameters from Table 1 to the model represented by equations (11-12), the double sinusoidal model for dry-band arc compression consists of:

$$i_a(t)=(-0.19L_a+1.41)\times\sin[0.408(t-1.12)] \times\{1-\text{sign}[(t-2.99L_a+2.28)(t-8.88)]\} \quad (13)$$

$$u_a(t)=12.3\sin(0.314t)\times\{1+\text{sign}[(t-2.99L_a+2.28)(t-8.88)]\} +4.35\times\{1-\text{sign}[(t-2.99L_a+2.28)(t-8.88)]\} \quad (14)$$

where: $i_a(t)$ and $u_a(t)$ are simulated current (mA) and voltage (kV) curves for a 10 ms half cycle. $i_a(t)$ and $u_a(t)$ are multiplied by -1 when $10 < t < 20$ (ms). Figure 9 shows the simulation results of I-V curves equivalent to results of Figure 3.

4 ANALYSIS

4.1 COMPARISON BETWEEN SIMULATED AND MEASURED I-V TRACES

Direct comparisons between simulated and measured I-V traces have been made to assess the accuracy of the double sinusoidal model. Figure 10 gives an example of a graphical comparison of measured data and simulation for the 1.7 cm arc. The correlation coefficient, r, between measurement and simulation is calculated in each case and presented in Table 2. The correlation coefficients are consistently high, confirming that the double sinusoidal model is appropriate in these cases.

Table 1. Details of model parameters

	Double Sinusoidal Model	
I-V curves [mA & kV]	$i_a(t)$	$u_a(t)$
Equation	(11)	(12)
U_a [kV]	—	17.4
I_a [mA]	$I_a=f(L_a)$	—
U_0 [kV]	—	8.7
ω_u [rad/ms]	0.314	0.314
ω_i [rad/ms]	0.408	—
t_1 [ms]	$t_1=f(L_a, t_2)$	$t_1=f(L_a, t_2)$
t_2 [ms]	8.88	8.88
L_a [cm]	$1.1<L_a<2.3$	$1.1<L_a<2.3$
t [ms]	$0<t<10$	$0<t<10$

Table 2. Correlation coefficients of current and voltage simulations.

Arc length (cm)	Correlation Coefficient	
	Voltage	Current
2.32	0.987	0.951
1.70	0.933	0.985
1.11	0.993	0.994

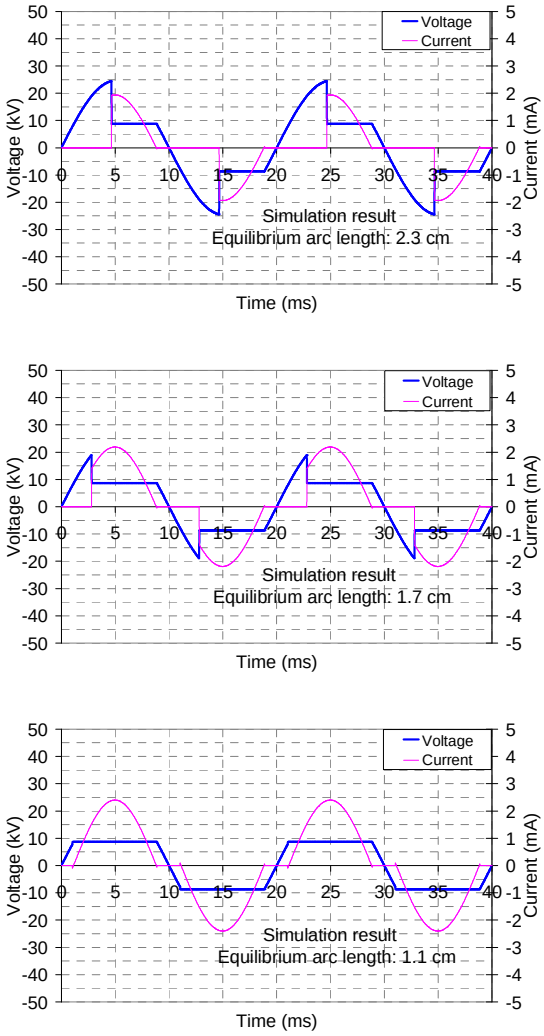

Figure 9. Simulation results of current and voltage traces.

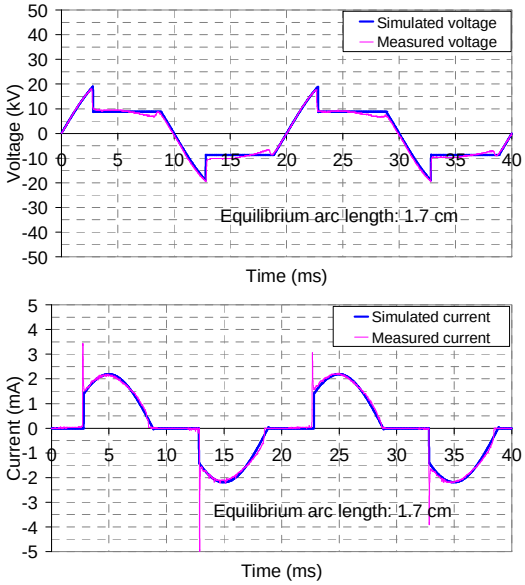

Figure 10. An example of comparison between simulated and measured I-V traces for an arc length of 1.7 cm

4.2 ARC RESISTANCE

Instantaneous arc resistance can be obtained by the ratio of arc voltage to arc current. Experimentally this is obtained from the measured voltage and current traces. In the double sinusoidal model, the instantaneous arc resistance (MΩ), $r_a(t)$, for times $t_1<t<t_2$ is simulated by using the $u_a(t)$ and $i_a(t)$ of equations (3) and (4), so that during the arcing period:

$$r_a(t)=\frac{u_a(t)}{i_a(t)}=\frac{U_0}{\sqrt{2}I_a\sin\omega_i[t-(\frac{\pi}{\omega_u}-t_2)]} \qquad (15)$$

By substituting the relevant model parameters from Table 1 we obtain,

$$r_a(t)=\frac{u_a(t)}{i_a(t)}=\frac{8.7}{(-0.38L_a+2.82)\sin[0.408(t-1.12)]} \qquad (16)$$

Figure 11 shows examples of both experiment and simulated arc resistances in different arc compression (dry-band length) situations. One characteristic of instantaneous arc resistance is its minimum value. This minimum resistance is located on the bottom of the 'U' shape in Figure 11 where the arcing current is greatest. Figure 12 summarizes the minimum arc resistance against slope angle for both experiment and simulation. Trend lines indicate that the more inclined the sample, the lower the arc resistance becomes. This results from the reduction of dry-band length: when the arc has been more compressed, the arc current peak increases (Figure 8) but the arc voltage does not change significantly with current.

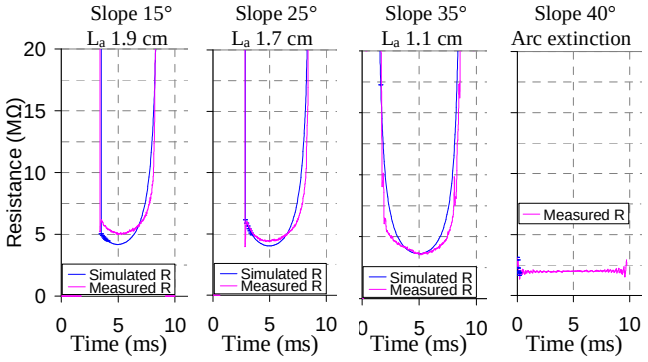

Figure 11. The instantaneous arc resistance from both experimental measurement and simulation work, for one half cycle (0 – 10 ms).

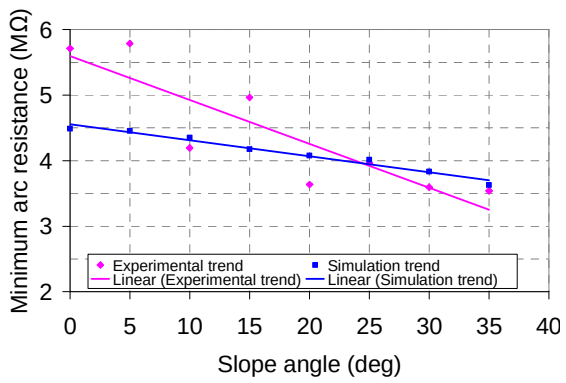

Figure 12. The relationship between minimum arc resistance and slope angle in both experimental case and simulation case.

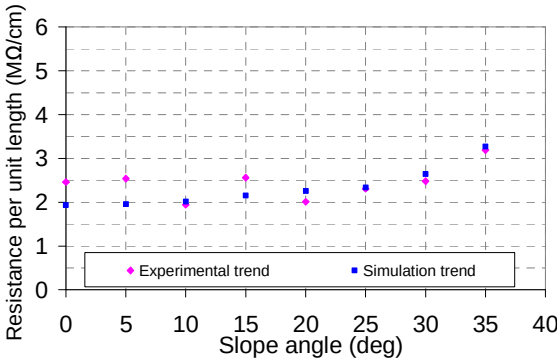

Figure 13. The relationship between minimum arc resistivity and slope angle.

The arc resistance per unit arc length also varies during the arcing period as a U shaped curve. The minimum value per half cycle as a function of slope angle is summarized in Figure 13. From both experiment and simulation, it is found that unlike the trend of resistance, the minimum arc resistance per unit length does not drop with the arc compression.

Clearly a significant improvement in the model of instantaneous resistance could be obtained by introducing a non-constant arcing voltage (instead of U_0). However, since the object of this study is the thermal characteristics of the arc, which are essentially averaged over repeated cycles, this was considered not to be necessary.

4.3 ARC POWER and ENERGY

Arc power is a significant characteristic which may lead to damage of insulator material. Based on the measured I-V traces, the arc powers of each half-cycle corresponding to different slope angles are calculated and shown in Figure 14. The result shows that the peak power for different arc lengths stays around 20 W and does not change too much. However, the arcing period increases with rod inclination.

For the experimental results, each half cycle of dry-band arcing has 800 measurement points. Based on these discrete data of arc power, the arc energy is calculated as:

$$E=\sum_{n=1}^{800}[P(t_n)+P(t_{n+1})]\times t_n/2 \qquad (17)$$

where E is the measured arc energy for a half cycle, $P(t_n)$ is the arc power (W) at the n^{th} sample point, and t_n is the interval sample time (0.025 ms).

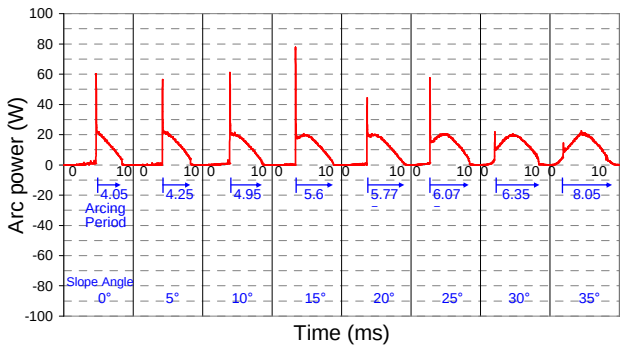

Figure 14. Arc power of different slope angles with variable arcing period.

Based on the simulated I-V waves, the accumulated arc energy for half a cycle of dry-band arc is calculated as:

$$E_a = \int_0^{\pi} u_a(t) i_a(t) dt \qquad (18)$$

where: E_a is the simulated arc energy (Joule) per half cycle, $i_a(t)$ is the simulated current wave, and $u_a(t)$ is the simulated voltage wave.

In both the pre-arcing ($0 < t < t_1$) and post-arcing ($t_2 < t < 10$) periods $i_a(t)$ is zero, which means there is no power dissipation during these two periods. As a result, the equation for arc energy calculated can be simplified as:

$$E_a = \int_{t_1}^{t_2} \{\sqrt{2} U_0 I_a \sin\omega_i [t - (\frac{\pi}{\omega_u} - t_2)]\} dt \qquad (19)$$

Substituting the model parameters from Table 1 into equation 19, the simulated arc energy for half a cycle of dry-band arcing is given by:

$$E_a = (-0.008 L_a + 0.06) \times [1 + \cos(-1.39 + 1.22 L_a)] \qquad (20)$$

The arc energy from the experimental results using equation (17) and the simulation result of equation (20) are sumarized and compared in Figure 15. In the situation of a dry-band being compressed in length, the reduction of arc length results in a rise in arc energy per half cycle.

The energy density, D, for each half cycle of dry-band arc can be calculated be dividing arcing energy by the dry-band area over which arcing occurs:

$$D = \frac{E}{2\pi R L_a} \quad (\text{Joule/m}^2) \qquad (21)$$

where R is the radius of sample rod, L_a is the arc length, and $2\pi RL_a$ is the dry-band area.

Figure 16 demonstrates the change of arc energy density with arc length from experimental and simulation results. The energy density increases by a factor of 6 with the reduction of arc length from 22 mm to 11 mm. This is due to the simultaneous rise of arc energy and the reduction of dry-band area during the arc compression.

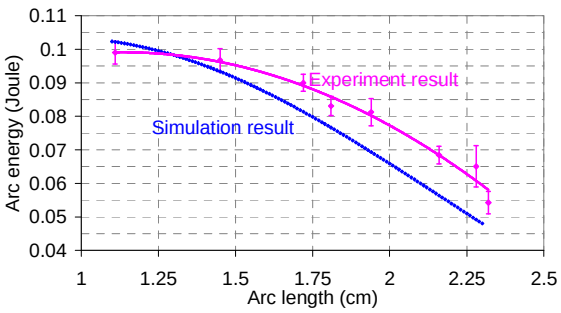

Figure 15. Experimental and simulation arc energy against arc length as a result of arc compression.

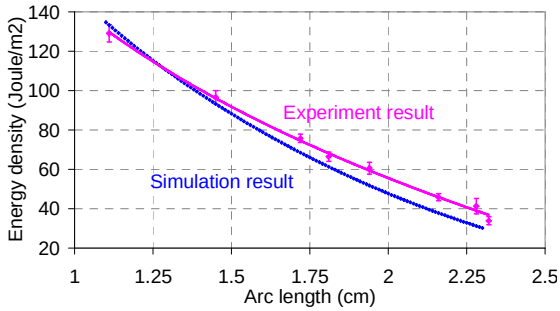

Figure 16. The relationship between arc length and energy density change.

5 CONCLUSIONS

An experimental study has been conducted to investigate the dry-band arcing on rod geometries, and has shown that stable arcs can be compressed in length by changing the angle of the rod to the horizontal. Such arcs remain stable and have been reduced in length by over 50%. The measured voltage and current waveforms have been modeled using a simple double sinusoidal model with a constant arc voltage. A notable feature of this model is that the time of extinction of the arcs during the power frequency cycle was independent of arc length. As the dry-band and its associated arc are reduced in length the duration of the arc during each half cycle increases, as the breakdown voltage of the dry-band is reduced. The minimum resistance of the arc is also reduced with the arc length leading to higher peak current as the arc length is diminished. As a result arc compression leads to higher arc energy, and in particular higher arc energy per unit area of dry-band. In the case studied here the arc energy per unit dry-band area was increased by a factor of 4 as a result of halving its length.

It is suggested that such dry-band arc compression processes may lead to more aggressive damage on the composite insulator surface, and could possibly accelerate the long-term aging effect into a short-term hazard. As a result, processes controlling insulation lifetime may not be continual and gradual, but are determined by events such as the occurrence of dry-band arc compression. Such event may be due to adventitious environmental circumstances, for example the combination of high pollution levels and wind.

Further study is required of the short-term unstable transient arc extinction process, since extrapolation of the arc length – power curve suggests rapidly increased energy density as the length reduces further beyond the stable conditions examined here. Moreover, geometrically the arc is closer to the rod surface as it becomes shorter, thereby further enhancing the transfer of power to the material – perhaps leading to even greater threat to the surface integrity.

ACKNOWLEDGMENTS

The authors would like to thank National Grid for their support in this work, and their permission to publish.

REFERENCES

[1] R. S. Gorur, E. A. Cherney and J. T. Burnham, Outdoor Insulators, ISBN 0-9677611-0-7, Phoenix, Arizona, USA, 1999.

[2] Y. Xiong, S. M. Rowland, J. Robertson and R. J. Day, "Surface Analysis of Asymmetrically Aged 400 kV Silicone Rubber Composite Insulators", IEEE Trans. Dielectr. Electr. Insul., Vol. 15, pp. 763-770, 2008.

[3] S. H. Kim, E. A. Chemey and R. Hackam, "Effect of Dry Band Arcing on the Surface of RTV Silicone Rubber Coatings", IEEE Intern. Sympos. Electr. Insul., Baltimore, MD, USA, pp. 237-240, 1992.

[4] Y. Zhu, M. Otsubo, N. Anami, C. Honda, O. Takenouchi, Y. Hashimoto, and A. Ohono, "Change of Polymeric Material Exposed to Dry Band Arc Discharge [Polymer Insulator Applications]", IEEE Conf. Electr. Insul. Dielectr. Phenomena (CEIDP), pp. 655-658, 2004.

[5] M. Kumosa, L. Kumosa and D. Armentrout, "Failure Analyses of Nonceramic Insulators Part 1: Brittle Fracture Characteristics", IEEE Electr. Insul. Mag., Vol. 21, No.3, pp. 14-27, 2005.

[6] S. Kumagai and N. Yoshimura, "Tracking and Erosion of HTV Silicone Rubber and Suppression Mechanism of ATH", IEEE Trans. Dielectr. Electr. Insul., Vol. 8, pp. 203-211, 2001.

[7] S. M. Rowland and I. V. Nichols, "The Effects of Dry-Band Arc Current on Ageing of Self-Supporting Dielectric Cables in High Fields", IEE Proc.- Sci. Meas. Technol, Vol. 143, pp. 10-14, 1996.

[8] S. M. Rowland and F. Easthope, "Electrical Ageing and Testing of Dielectric, Self-Supporting Cables for Overhead Power Lines", Proc. IEE Part A, Vol. 140, pp. 351-356, 1993.

[9] G. G. Karady, S. Baozhuang, H. Qi, D. Srinivasan and M. W. Tuominen, "Experimental Investigation of the Aging Process on ADSS Optical Fiber Cables", IEEE Power Engineering Soc. Summer General Meeting, pp. 225-228, 2003.

[10] S. Baozhuang, G. G. Karady, H. Qi and M. W. Tuominen, "Experimental Studies of the Characteristics of Dry Band Arcing on ADSS Fiber Optic Cables", IEEE Trans. Power Delivery, Vol. 19, pp. 1936-1940, 2004.

[11] S. Baozhuang, H. Qi, G. G. Karady and M. W. Tuominen, "Studies on the Length of Dry Band Arcs on ADSS Fiber Optic Cables", IEEE Conf. Electr. Insul. Dielectr. Phenomena (CEIDP), pp. 353-356, 2003.

[12] H. Qi, S. Baozhuang, G. G. Karady and M. Tuominen, "Study on the Effect of Test Circuit Parameters on Dry Band Arcing Failure of ADSS Fiber Optic Cable", IEEE Power Engineering Soc. Summer General Meeting, pp. 207-210, 2003.

[13] Q. Huang, G. G. Karady, B. Shi and M. Tuorninen, "Calculation of the Electric Field Distribution on ADSS Fiber Optic Cable", IEEE Conf. Electr. Insul. Dielectr. Phenomena (CEIDP), pp. 379-382, 2003

[14] L. H. Meyer, S. H. Jayaram and E. A. Cherney, "Correlation of Damage, Dry Band Arcing Energy, and Temperature in Inclined Plane Testing of Silicone Rubber for Outdoor Insulation", IEEE Trans. Dielectr. Electr. Insul., Vol. 11, pp. 424-432, 2004.

[15] X. Zhang, S. M. Rowland and V. Terzija, "Modelling of Dry-Band Arc Compression", Accepted for publication in 16th International Symposium on High Voltage Engineering, 2009.

[16] H. Qi, G. G. Karady, B. Shi and M. Tuominen, "Numerical Simulation of Dry-Band Arcing on the Surface of ADSS Fiber Optic Cable", IEEE Trans. Dielectr. Electr. Insul., Vol. 12, pp. 496-503, 2005.

Xin Zhang was born in Jinan, China. He completed the B.Eng. degree in automation at Shandong University in 2006, and received the M.Sc. degree with distinction in electrical power engineering from the University of Manchester in 2007. He is currently studying for his Ph.D. degree in electrical power engineering at the National Grid High Voltage Research Center in the same University.

Simon M. Rowland (SM'07) was born in London, England. He completed the B.Sc. degree in physics at UEA and the Ph.D. degree at London University. He was awarded the IEE Duddell Premium in 1994 and became a FIEE in 2000. He has worked for many years on dielectrics and their applications. He has also been Operations and Technical Director multinational manufacturing companies. He joined The School of Electrical and Electronic Engineering in The University of Manchester as a Senior Lecturer in 2003 and was appointed Professor of Electrical Materials in 2009. He is Vice-President Admin. of the IEEE Dielectric and Electrical Insulation Society.

Vladimir Terzija (M'95-SM'00) is the EPSRC Chair Professor in Power System Engineering in the School of Electrical and Electronic Engineering, The University of Manchester, where he has been since 2006. From 1997 to 1999, he was an Assistant Professor at the University of Belgrade. In 1999, he was awarded a prestigious Humboldt Research Fellowship. From 2000 to 2006, he was with ABB AG, Germany, as an expert for switchgears and distribution automation. His main research interests are application of intelligent methods to power system monitoring, control, and protection, switchgear, and DSP applications in power systems.